September 2008
SLAC-PUB-13395

OBSERVATION OF COHERENT OPTICAL TRANSITION RADIATION IN THE LCLS LINAC*

H. Loos†, R. Akre, A. Brachmann, F.-J. Decker, Y. Ding, D. Dowell, P. Emma, J. Frisch, S. Gilevich, G. Hays, Ph. Hering, Z. Huang, R. Iverson, C. Limborg-Deprey, A. Miahnahri, S. Molloy, H.-D. Nuhn, J. Turner, J. Welch, W. White, J. Wu, SLAC, Menlo Park, CA 94025, USA
D. Ratner, Stanford University, Stanford, CA 94305, USA

Abstract

The beam diagnostics in the linac for the Linac Coherent Light Source (LCLS) X-ray FEL project at SLAC includes optical transition radiation (OTR) screens for measurements of transverse and longitudinal beam properties. We report on observations of coherent light emission from the OTR screens (COTR) at visible wavelengths from the uncompressed and compressed electron beam at various stages in the accelerator.

INTRODUCTION

The use of optical transition radiation (OTR) as a transverse electron beam diagnostic for linear accelerators is very attractive [1]. Transition radiation provides an instantaneous visible light signal that has a linear response to the beam density and can conveniently be detected with an imaging system. The efficiency in terms of number of photons per electron is usually of the order of $10^{-3} - 10^{-2}$ and has only a logarithmic dependence on the beam energy. The resolution is only limited by the imaging optics and beam sizes as small as $5\,\mu$m have been observed [2].

The linear response of the light intensity to the transverse charge density is a result of the incoherent superposition of the radiation from individual particles with random phase correlations at visible wavelengths within the length of the electron bunch. This normally applies to accelerators with bunch lengths ranging from millimeters to tens of micrometers. The presence of microstructure at visible wavelengths in an electron beam however can generate coherent optical transition radiation (COTR) and was previously reported for a beam modulated by a visible FEL [3] and a beam generated by laser-plasma interaction [4].

In the case of ultra-bright, low emittance electron beams originating from laser-driven RF guns like the LCLS accelerator, micro-structure at visible wavelengths can be generated in the uncompressed and compressed electron bunches. The effects of coherent light emission from such bunches can both give insight into the longitudinal dynamics of the beam acceleration but also compromise the use of OTR as a transverse beam diagnostic.

* Work supported by US DOE contract DE-AC02-76SF00515.
† loos@slac.stanford.edu

LCLS ACCELERATOR

The LCLS accelerator (Fig. 1) serves as the driver for the X-ray free electron laser and provides a high brightness electron beam. The first part of the accelerator consists of a 6 MeV photocathode RF-gun driven by a frequency tripled Ti:Sapphire laser at 255 nm that generates a bunch charge of up to 1 nC with beam emittances around or below $1\,\mu$m. The beam is subsequently accelerated in four stages (labeled L0, L1, L2, and L3) to energies up to 135 MeV, 250 MeV, 4.3 GeV, and 14 GeV. Of the four bend magnet systems, the first (DL1) is a dogleg system to insert the beam from the injector tunnel into the main linac, whereas the next two (BC1 and BC2) are magnetic chicanes to compress the bunch length from initially $800\,\mu$m to $200\,\mu$m and $25\,\mu$m, respectively. The final bend (BSY) is presently utilized as an energy spectrometer. A quadrupole magnet (QB) in the first dogleg enables the dispersion downstream of the dogleg to be canceled.

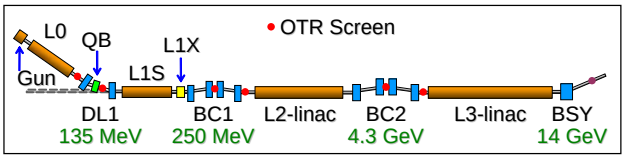

Figure 1: Layout of the LCLS accelerator.

Diagnostics using OTR are implemented at various stages of the LCLS accelerator, namely after the first acceleration section (labeled OTR2), in the first dogleg (OTR4), and both within (OTR11 and OTR21) and after (OTR12 and OTR22) the magnetic chicanes. The diagnostics consist of a $1\,\mu$m thick aluminum foil oriented at 45 degrees to the beam, two insertable neutral density filters, a telecentric lens with numerical aperture of 0.18 and working distance of 160 mm, and a mega-pixel CCD camera with a 0.42 magnification giving a calibration of 11 pixels per μm in the object plane. The CCD has a 12-bit digitizer with an effective signal to noise ratio of 1000.

OTR IMAGE FORMATION OF COHERENT ELECTRON BUNCHES

The imaging of objects with an optical system onto a view screen is usually described in terms of the point spread function (PSF) which is the intensity distribution of

Invited talk/Presented at the 30th International Free Electron Laser Conference, 8/24/2008 to 8/29/2008, Gyeongju, Korea

a point source in the image plane. In the case of OTR, the source distribution is given by the pseudo-photon distribution of the beam's coulomb field which is reflected off the transition radiator. Using Fraunhofer diffraction theory, the field distribution in the image plane can be quite accurately described as a convolution of the source field with the diffraction pattern of the lens aperture of the imaging optics with the PSF as the respective intensity distribution. The OTR image of an entire beam is obtained as the convolution of the PSF with the transverse particle distribution. This description is no longer accurate if the particles in the bunch have a phase correlation at optical wavelengths. In this case, the field distribution and polarization rather than the PSF of OTR has to be considered.

The transverse pseudo-photon electric field distribution which represents the source of the transition radiation, is given for an angular frequency $k = \omega/c$ by [5]

$$\mathbf{E}\left(\mathbf{r}\right) = -\frac{q}{\pi v}\frac{\mathbf{r}}{r}\alpha K_1\left(\alpha r\right) \ , \tag{1}$$

$$\widetilde{\mathbf{E}}\left(\boldsymbol{\kappa}\right) = \frac{1}{2\pi}\frac{iq}{\pi v}\frac{\boldsymbol{\kappa}}{\kappa^2+\alpha^2} \tag{2}$$

in real and transverse frequency space with $\alpha = k/(\beta\gamma)$. The imaging of this distribution by a lens of radius d at a distance z_l onto a screen leads to the expression for the electric field on the screen

$$\mathbf{E}_S\left(\mathbf{r}\right) = \int^{kd/z_l} d^2\kappa\, e^{i\boldsymbol{\kappa}\mathbf{r}}\,\widetilde{\mathbf{E}}\left(\boldsymbol{\kappa}\right) \ , \tag{3}$$

assuming unit magnification for simplicity. For $d/z_l \gg 1/\gamma$a good approximation is given by [6]

$$\mathbf{E}_S\left(\mathbf{r}\right) = -\frac{q}{\pi v}\frac{\mathbf{r}}{r}\left[\alpha K_1\left(\alpha r\right) - \frac{1}{r}J_0\left(krd/z_l\right)\right] \ . \tag{4}$$

Figure 2 shows the PSF as the absolute square of the source field of Eq. (1), the approximation of the PSF on the screen from the absolute square of Eq. (4) for $\gamma = 500$, an acceptance angle θ of the lens of 75 mrad and a wavelength of 1 μm. The FWHM of the PSF is $1.44\lambda/\theta$ [7].

The image formed by the radiation from an entire bunch of N electrons is obtained from the superposition of the fields from each particle at locations $\mathbf{r}_j$ and z_j as

$$\mathbf{E}_{S,N}\left(\mathbf{r}\right) = \sum_j e^{-ikz_j}\mathbf{E}_S\left(\mathbf{r}-\mathbf{r}_j\right) \ . \tag{5}$$

Taking the absolute square for the intensity distribution, the sum in Eq. (5) splits into an incoherent part independent of the longitudinal positions and proportional to N and a coherent part depending on the z coordinates and proportional to N^2. For large N the two sums can be expressed as integrals over the normalized particle distribution $\rho\left(\mathbf{r}', z\right)$ giving

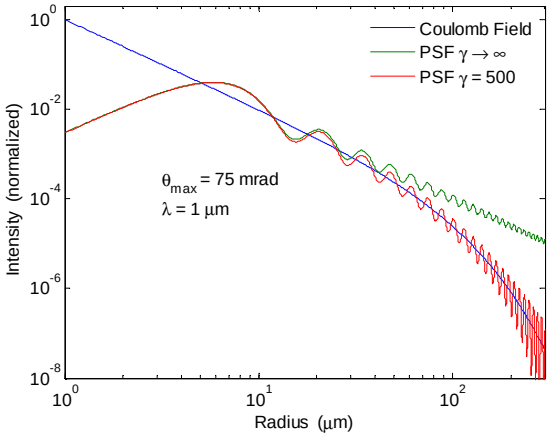

Figure 2: Point spread function of the OTR source distribution for a lens acceptance angle of 75 mrad. Shown are the Coulomb field for $\gamma = 500$ and the PSF at the same γ and for $\gamma \to \infty$.

$$\left|\mathbf{E}_{S,N}\left(\mathbf{r}\right)\right|^2 = N\int d^2r'dz\,\rho\left(\mathbf{r}',z\right)\left|\mathbf{E}_S\left(\mathbf{r}-\mathbf{r}'\right)\right|^2 + N^2\left|\int d^2r'dz\,e^{-ikz}\rho\left(\mathbf{r}',z\right)\mathbf{E}_S\left(\mathbf{r}-\mathbf{r}'\right)\right|^2 \ . \tag{6}$$

The first integral represents the incoherent OTR imaging as the convolution of the PSF with the transverse distribution, whereas the second integral contains the convolution of the single particle field $\mathbf{E}_S$ at the screen with the frequency component at wavenumber k of the density function ρ. The second integral, the coherent electric field distribution on the screen, can be written as

$$\mathbf{E}_{C,N}\left(\mathbf{r}\right) = 2\pi\frac{Nq}{i\pi v}\int^{kd/z_l} d^2\kappa\,\rho\left(\boldsymbol{\kappa},k\right)\frac{\boldsymbol{\kappa}e^{i\boldsymbol{\kappa}\mathbf{r}}}{\kappa^2+\alpha^2} \tag{7}$$

with $\rho\left(\boldsymbol{\kappa},k\right)$ the spatial frequency distribution of the density function at wavenumber k. If the maximum spatial frequencies κ_{max} of the beam distribution are smaller than the integration limit and also smaller than k/γ, then the denominator in Eq. (7) can be approximated with α^2 and the entire expression is a Fourier integral of the gradient operator. The field then becomes

$$\mathbf{E}_{C,N}\left(\mathbf{r}\right) = -2\pi\frac{Nq}{\pi v}\frac{\gamma^2\beta^2}{k^2}\nabla\rho\left(\mathbf{r}\right) \ . \tag{8}$$

If the electron beam has full transverse coherence at visible wavelengths and the beam size is large compared to $\lambda\gamma$, the OTR image of the beam will not show the beam distribution, but the absolute square of the gradient of the transverse beam shape. For a beam with circular symmetry, the COTR image will show a ring structure. In the limit of a very small beam size, ρ becomes unitiy in Eq. (7) and the COTR image will be the PSF.

OBSERVATIONS OF COTR

A number of different observations with the OTR diagnostics at different stages of the LCLS indicate the presence of coherent OTR and will be discussed in the following sections.

COTR of Uncompressed Bunches

The intensity and transverse size of the OTR image of the electron beam at a diagnostics (OTR12) downstream of the first bunch compressor (BC1) were measured as a function of the strength of the quadrupole in the first dogleg and are shown in Fig. 3. The bunch compressor was turned off during the measurement giving an uncompressed bunch length of about 800 μm at a bunch charge of 1 nC. The quadrupole cancels the dispersion of the dogleg at its nominal value of 10.8 kG. The light intensity increases up to a factor of 4 within a narrow range of 0.1 kG about the nominal quadrupole strength. Both the horizontal and vertical beam size change by up to 25%. The drive laser can be excluded as a source of such temporal structure at visible wavelengths in the beam, as the utilized bandwidth of the laser oscillator of 3 nm only supports modulation wavelengths larger than 150 μm. The source of the longitudinal structure generating this coherent enhancement is rather assumed to be the longitudinal space charge instability which creates an energy modulation at visible wavelengths in the beam upstream of DL1. In this part of the injector before any bend magnets, no coherent effects on the OTR screens located there could be observed. The small R_{56} of the dogleg converts the energy modulation into a temporal structure. At values other than the nominal strength for the QB magnet, the finite R_{51} and R_{52} elements tilts the phase front of the modulation in the $x - z$ plane and suppress the coherence.

The fact that the OTR image shape remains nearly Gaussian and only the size changes, and that the enhancement factor is only about 4, indicate that only a very small fraction of the beam radiates coherently and is localized randomly at many positions in the beam. A detailed analysis of the micro-bunching observations can be found in [8].

The dependency of the OTR light intensity on the bunch charge was measured under the same conditions on OTR12 with no bunch compression. As an incoherent reference, the OTR foil in the dispersive section of the bunch compressor was inserted into the beam which increases both angular and energy spread and suppresses the coherence. The measurement and fits are shown in Fig. 4. A linear fit to the incoherent CCD counts C to the number of electrons N gives the diagnostics efficiency η from $C = \eta N$. The coherent data is well described up to about 3×10^9 electrons with a fit including a quadratic term $C = \eta N + \eta N^2 r^2$ with r as the bunch form factor within the spectral range of the CCD. Figure 5 shows this coherent fraction r against the charge. At low charge the fraction remains almost constant at 3×10^{-5}, but drops off above 3×10^9 electrons as the higher charge generates a larger slice energy spread that reduces the micro-bunching gain.

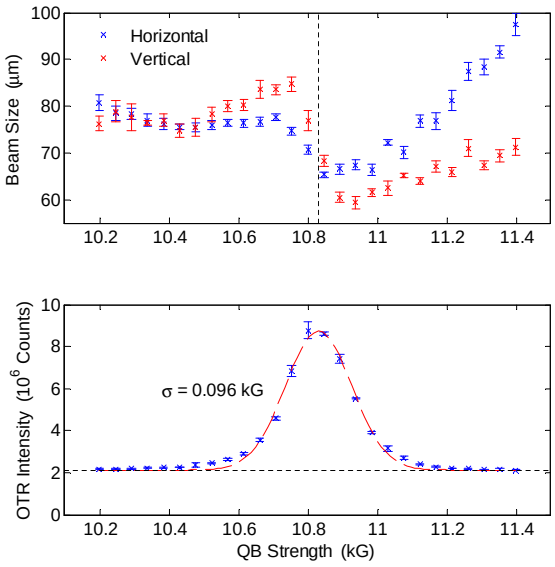

Figure 3: OTR intensity (lower) and beam sizes (upper part) measured downstream of BC1 at OTR12 as a function of the dispersion correction quadrupole (QB) in the first dogleg with no bunch compression. The vertical line indicates the peak of the OTR intensity curve.

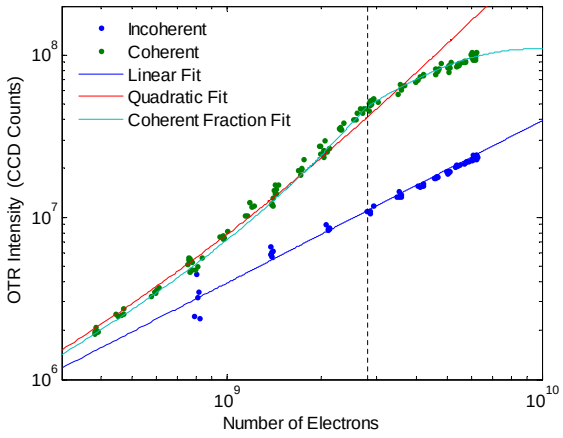

Figure 4: Dependency of OTR light intensity on the bunch charge. The data shown is for 250 MeV and uncompressed bunches. The coherent fraction fit uses the fit from Fig. 5.

COTR Spectra of Compressed Bunches

A transmission grating installed in one of the insertable filter holders close to the camera lens enables a low resolution measurement of the visible OTR spectrum at several diagnostics stations. With a calibration of 103 nm/mm a spectral resolution below 10 nm can be achieved with typical beam sizes below 100 μm. OTR spectra of the compressed beam after BC1 for a charge of 250 pC and nominal

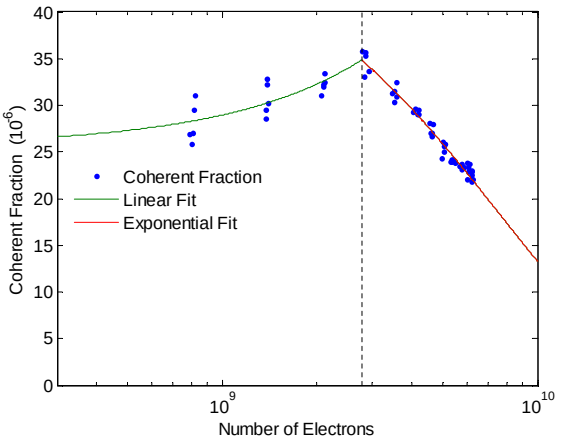

Figure 5: Fraction of the bunch charge radiating coherently as a function of charge. A linear and an exponential fit are used below and above 2.8×10^9 electrons.

bunch length of 60 μm and an incoherent reference spectrum are shown in the upper part of Fig. 6. The lower part shows the spectral gain as the ratio of the coherent and the incoherent spectrum. The enhancement is present over the entire visible range with a gain close to 1 at the blue end and a much larger gain towards the infrared. The width of the spikes in the spectra of about 6 nm equals the spectral resolution given by the beam size and indicates the presence of very narrow spectral features. The detailed structure of the spectra and location of the spikes fluctuate from shot to shot.

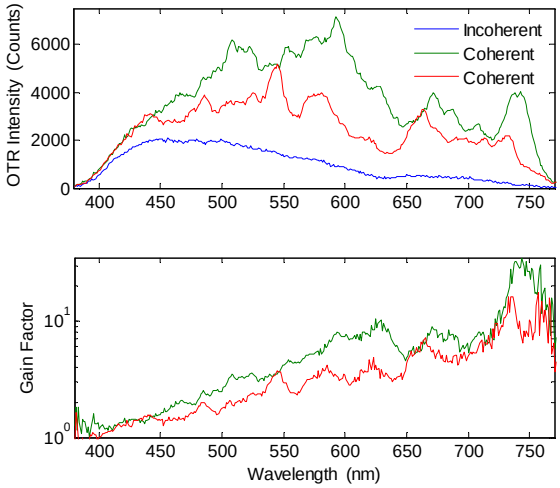

Figure 6: OTR light spectra after BC1 with the beam under normal compression (red and green) and with the coherence suppressed (blue). The spectra are in the upper panel and the spectral gain factor (ratio of coherent to incoherent spectrum) in the lower one.

COTR Images of Compressed Bunches

The OTR images from the ultrashort, highly compressed bunches after the first and second bunch compressor show a large coherent enhancement factor of up to 10^2 after BC1 and up to 10^5 after BC2 and exhibit complex and varying transverse structures indicating a high degree of longitudinal and transverse coherence. One example of a ring structure shown in Fig. 7 was taken after BC2 at a charge of 250 pC and nominal bunch length of about 10 μm. The light intensity is enhanced by a factor of 1000. A simulation of the COTR image using the second term in Eq. (6) is also included in the figure. The actual beam size at the OTR screen is not known and is estimated from the design lattice and the normalized emittance of 0.7 μm to be 70 μm. For the simulation, a size of 100 μm was selected to better fit the measurement. The Gaussian beam distribution shown in the upper right of the figure assuming full transverse coherence was then convoluted with the single particle field distribution on the OTR screen from Eq. (4) whose bipolar horizontal field component is shown in the upper left. Most of the positive and negative parts of the field cancel in the convolution and result in a ring structure in the lower left.

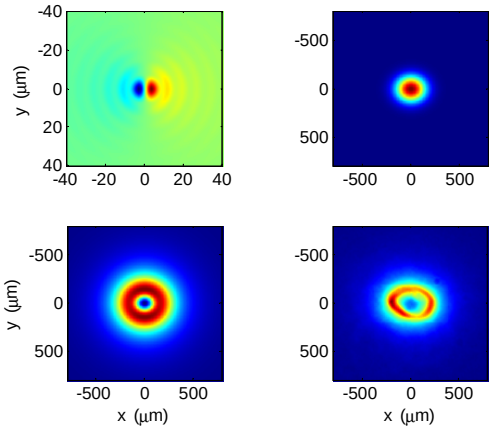

Figure 7: Simulation of COTR image. Upper panel left is the horizontal component of the source field, right is the beam distribution, lower panel left is the simulated COTR image and right the measured image.

The horizontal cross-section of the measurement and the simulation can be compared in Fig. 8. The long tails agree well, while the peaks are narrower in the measured data than in the simulation. This indicates a non-Gaussian distribution with steeper edges. The measured data also does not drop to zero in the center which might be due to parts of the bunch radiating with small transverse coherence.

The transverse spectral distribution of the OTR light can be measured with a color CCD camera. Figure 9 shows a more complicated COTR shape with two rings and a variation in color across the image. The simulation shown in the lower part of the figure was done similarly to the previous one but with a simulated particle distribution at the screen

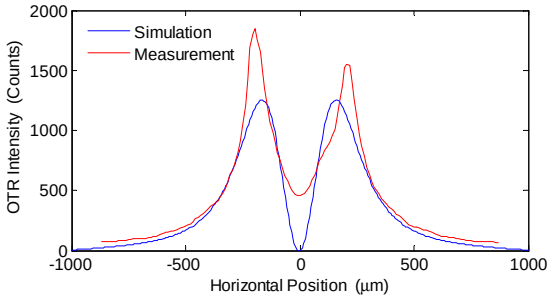

Figure 8: Horizontal lineout across the center of the COTR distributions in Fig. 7.

location [9] using 10^6 particles in Elegant for tracking. The COTR distribution at a given wavelength was calculated by summing up the phases of all particles within every transverse bin and then convolving it with the OTR field distribution. This was done for 11 different wavelengths across the visible range and the images combined into a color image. The two rings with different color are generated by the two current peaks at the head and tail of the bunch. The CSR energy loss in BC2 moves the tail to the right as visible in both in the measurement and the simulated image.

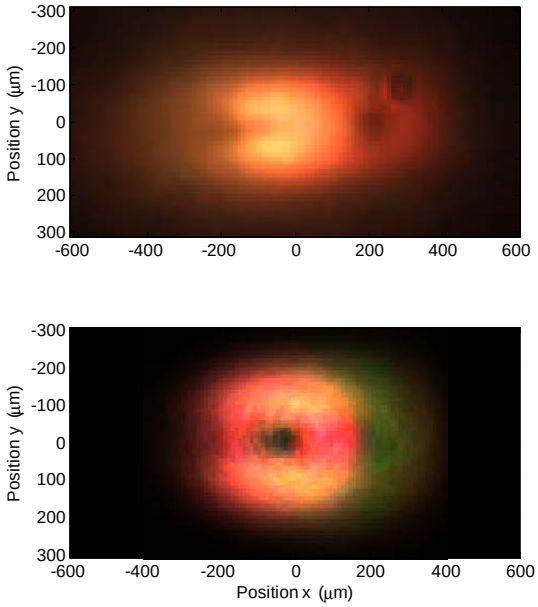

Figure 9: Comparison of observed and simulated COTR color images.

The spectral content of the COTR is fluctuating from shot to shot, but for transversely coherent beams the spectrum can be quite uniform across the beam. This is shown in Fig. 10 where the shape of the COTR distribution is steady and only the color changes from shot to shot.

In summary, coherence effects in OTR have been observed for both uncompressed and compressed electron bunches in the increase of light intensity, in the change of the spectral distribution, as well as in the transverse shape of the beam image. The enhancement seen for uncompressed bunches is contributed to the amplification of shot-noise in the beam due to a micro-bunching instability. The effect for compressed beams as supported by simulations is attributed to both a shift of long wavelength micro-structure into the visible and the generation of micron-length spikes in the compression process.

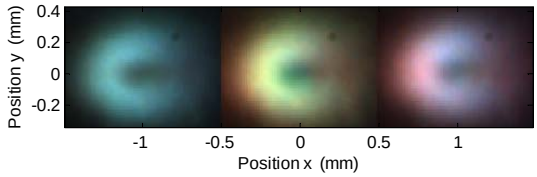

Figure 10: Series of COTR color images taken within one minute showing varying color content from shot to shot.

These effects compromise the use of OTR as a reliable beam diagnostics beyond the injector due to the high brightness, i.e. small transverse and longitudinal emittance, of the beam and will impact other high brightness electron accelerators for X-ray FELs besides LCLS. A possible mitigation for the coherence effects will be be upcoming installation of a laser heater which increases the energy spread in the injector from 3 keV up to 30 keV in order to suppress CSR effects in the bunch compressors. Spectral and spatial filtering methods seem less feasible due to the coherent enhancement over the entire visible spectrum, the small transverse coherence length for uncompressed bunches, and the large enhancement factor of several orders of magnitude. A dedicated COTR experimental station is planned to be installed for the next run of the LCLS.

ACKNOWLEDGEMENTS

We wish to thank R. Fiorito for many fruitful discussions on optical transition radiation.

REFERENCES

[1] D. W. Rule, R. B. Fiorito, Accelerator Instrumentation, BNL, AIP Conf. Proc. 229, p. 315 (1991).

[2] M. Ross, *et al.*, BIW 2002, BNL, AIP Conf. Proc. 648, p. 237 (2002).

[3] A. H. Lumpkin, *et al.*, Phys. Rev. Lett. 88 (2002) 234801.

[4] Y. Glinec, *et al.*, Phys. Rev. Lett. 98 (2007) 194801.

[5] J. D. Jackson, *Classical Electrodynamics* (J. Wiley & Sons, New York, 1962, 1975).

[6] D. Xiang, W.-H. Huang, Y.-Z. Lin, Phys. Rev. STAB 10 (2007) 062801.

[7] V. A. Lebedev, Nucl. Instrum. Meth. A 372 (1996) 344.

[8] D. Ratner, A. Chao, Z. Huang, these proceedings.

[9] Y. Ding, private communication.